journal

J. Am. Ceram. Soc., 86 [9] 1586–91 (2003)

Formation of β-Silicon Nitride Crystals from (Si,Al,Mg,Y)(O,N) Liquid: II, Population Dynamics and Coarsening Kinetics

Lingling Wang* and Tseng-Ying Tien*

Department of Materials Science and Engineering, University of Michigan, Ann Arbor, Michigan 48109-2136

I-Wei Chen*

Department of Materials Science and Engineering, University of Pennsylvania, Philadelphia, Pennsylvania 19104-6272

Precipitation, growth, and coarsening of Si_3N_4 crystals in (Si,Al,Mg,Y)(O,N) liquids at 1680°C has been studied. Contrary to the common observation in kinetics, coarsening rates of crystals in length and width are found to accelerate when the total volume of crystals remains little changed. This is attributed to the concomitant β-Si_3N_4 to β′-SiAlON transformation, which introduces an additional driving force for crystal dissolution and reprecipitation. As a result of the additional driving force, which has a nonmonotonic size dependence, the normalized size distribution is expected to evolve with time, initially broadening, then shifting skewing as the transformation passes the midpoint, and finally converging to a sharp distribution as the transformation completes. These evolutions have been observed in all the compositions studied.

I. Introduction

In the preceding paper (Part I),[1] we show that the populations of rodlike crystals in several silicon nitride (Si_3N_4) systems undergo an evolution that is reminiscent of nucleation, growth, and coarsening. During the nucleation stage, the crystal population increases, whereas, during the coarsening stage, the crystal population decreases. The nucleation stage and the follow-up growth stage (during which the population remains constant), however, are relatively short in our experiments. Therefore, most of our kinetic data fall into the coarsening stage. The coarsening stage is important for practical reasons, because most Si_3N_4 ceramics are prepared in a time–temperature range when extensive coarsening takes place.

Classical theories of crystal coarsening of Lifshitz, Slyozov, and Wagner (LSW)[2,3] predict decreasing coarsening rates with time. Over the past 50 years, there has been very extensive discussion of the validity of these theories.[4–8] The general conclusion is that the predicted time dependence of decreasing coarsening rate seems to be valid, but the predicted size distribution by the LSW model is rarely realized. There is also a disagreement regarding the effect of volume fraction, recognizing that coarsening experiments are never performed in the dilute limit envisioned in the LSW model. In Si_3N_4 ceramics, a decreasing coarsening rate appears to apply to the data of Hwang and co-workers[9,10] and Lai and Tien[11] Nevertheless, the time exponents they have obtained are different from those predicted by the LSW theory. This discrepancy is attributed to the growth anisotropy of hexagonal rodlike crystals of Si_3N_4 and, possibly, the different extent of interface kinetic control on different facets.

The above Si_3N_4 data have been obtained from ceramics in which crystal impingement is commonplace. Using samples with a lower volume fraction of Si_3N_4 crystals that are relatively free of impingement, Krämer *et al.*[12,13] have observed a constant growth velocity along the length direction and no growth in the width direction. Their velocity data,[12] however, were collected during the growth stage (increasing β-Si_3N_4 volume fraction and decreasing but still substantial α-Si_3N_4). Therefore, it is not clear whether the conclusion is applicable to the coarsening stage (constant β volume fraction with no α). We have also examined several Si_3N_4 systems in which impingement is absent. The data of average linear dimension presented in Part I (Fig. 4 therein) suggest that the coarsening rate may actually accelerate with time. This unusual feature never has been reported in the literature of particle/microstructure coarsening, although some evidence of such behavior is present in the work of Krämer *et al.*, but not emphasized. (We refer to Fig. 6(b) of Ref. 13, which shows, at 1640°C, a concave upward feature in the data of mean crystal diameter versus time. A concave downward feature in the plot of dimension versus time should have been expected for a decreasing coarsening rate.)

As mentioned above, the data analysis of Krämer *et al.* focuses on the earlier stage, in particular, when the α to β transformation is concomitant with β/β′ crystallization and when Al/O precipitation is less significant. To obtain a broader picture, we have conducted experiments that extend to a kinetic range wide enough to make an assessment of the coarsening stage and the influence of β-Si_3N_4 to β′-SiAlON conversion.[1] This assessment is based on the detailed population statistics presented here. An analysis of the time evolution of the data leads to the growth velocity, which provides a direct evidence of the coarsening dynamics—small crystals shrinking while large ones growing. The effect of phase conversion is also shown to lead to accelerated coarsening of Si_3N_4 crystals.

II. Experimental Procedures

Our experiments used the same samples as in Part I, and the crystal statistics were collected following the same procedures.[1] Briefly, four different compositions, designated as CY1 to CY4, were investigated following isothermal heat treatment (1680°C) at different times (up to 4 h). These compositions had approximately the same O/N ratio and the same Al/Y/Mg ratio, with the main difference being the Si/(Al,Y,Mg) ratio, which increased from CY1 to CY4. The amount of β-Si_3N_4/β′-SiAlON crystals that eventually precipitated from the liquid was ~15%. Phase analysis

R. Riedel—contributing editor

Manuscript No. 186716. Received August 22, 2002; approved April 14, 2003.

Supported by the U.S. Department of Energy, under Contract No. DE-AC05–84OR22464, and by the Air Force Office of Scientific Research, under Grant No. AFOSR-G-F49620–01-1–0150. Facilities at the University of Pennsylvania are supported by the U.S. National Science Foundation under MRSEC Grant No. DMR-00-79909.

*Member, American Ceramic Society.

using X-ray diffractometry (XRD) identified a trend of compositional evolution from β-Si_3N_4 to β′-SiAlON during the course of our experiments, without a major increase of the volume fraction of the crystals. Scanning electron microscopy (SEM) was used for microstructure characterization. Dimensions of β/β′ crystals were determined using SEM in the secondary electron mode. To aid measurement, polished samples were chemically etched using molten alkali hydroxides. The SEM images revealed the hexagonal rod shape of Si_3N_4 crystals. For quantitative analysis of dimensions (length *L* and width *W*), only crystals with both ends visible and at least two side surfaces fully exposed were included. The width measured was either the span between two adjacent side surfaces or the span between three adjacent side surfaces. Statistically, the measurement yielded a value very close to the diameter of an equivalent circle that has the same area as the cross section of a hexagonal rod. Further details of the above experimental procedures were described in Part I.

III. Results

We shall use length distributions shown in Figs. 1(a)–(d) to illustrate the data available from our experiments. The cumulative distributions of the lengths of crystals of CY1 at five various times are shown in Fig. 1(a). The distributions are rather smooth, indicating good statistics. The differential distribution, which is the (negative) first derivative of the cumulative distribution, is shown in Fig. 1(b). The differential distributions are typically bimodal; indeed, they can be fitted with two Gaussian functions, with a correlation factor of >0.98. One such fitted curve is shown in Fig. 1(b) for illustration. The size ranges of the above distributions generally grow with time, but the total numbers of crystals decrease over time. This number, per volume, is the crystal concentration that is reported in Part I (Fig. 5 therein.) We use the crystal concentration at 16 min as the reference and assign a weight factor that is the ratio of the concentration at time *t* to the concentration at 16 min. We then multiply this weight factor to the distribution and obtain the concentration-weighted cumulative distribution *F* shown in Fig. 1(c). The corresponding concentration-weighted differential distributions are shown in Fig. 1(d).

To compare differential distributions at different times, we normalize them by the mean length and plot the resultant distributions in Figs. 2(a) and (b) for two compositions, CY1 and CY4. (These two compositions represent the extremes of our data. The differential distributions of CY2 and CY3, which are very similar, lie in between these extremes. The distributions of CY2 have been shown elsewhere to compare with the prediction of a coarsening model.[14]) As mentioned before, these distributions tend to be bimodal. The distributions at 16 min are almost centered, and they are slightly skewed toward the smaller size. This skewing is consistent with the notion of continuous crystal nucleation, leaving a large population at small sizes. Later, the bimodal feature becomes more prominent. The weight of the first mode (with shorter lengths) is initially larger than that of the second mode (with longer lengths), and, as time progresses, this trend is reversed. Remarkably, at 256 min, the distributions sharpen significantly and become unimodal again. These distributions all differ in some way from the LSW prediction, which states that the normalized distribution is time invariant and skewed to the right, having a peak frequency of ~2.2.[2,3] (Interface control lowers the peak frequency but retains the invariance and the rightward skewing.[3,15])

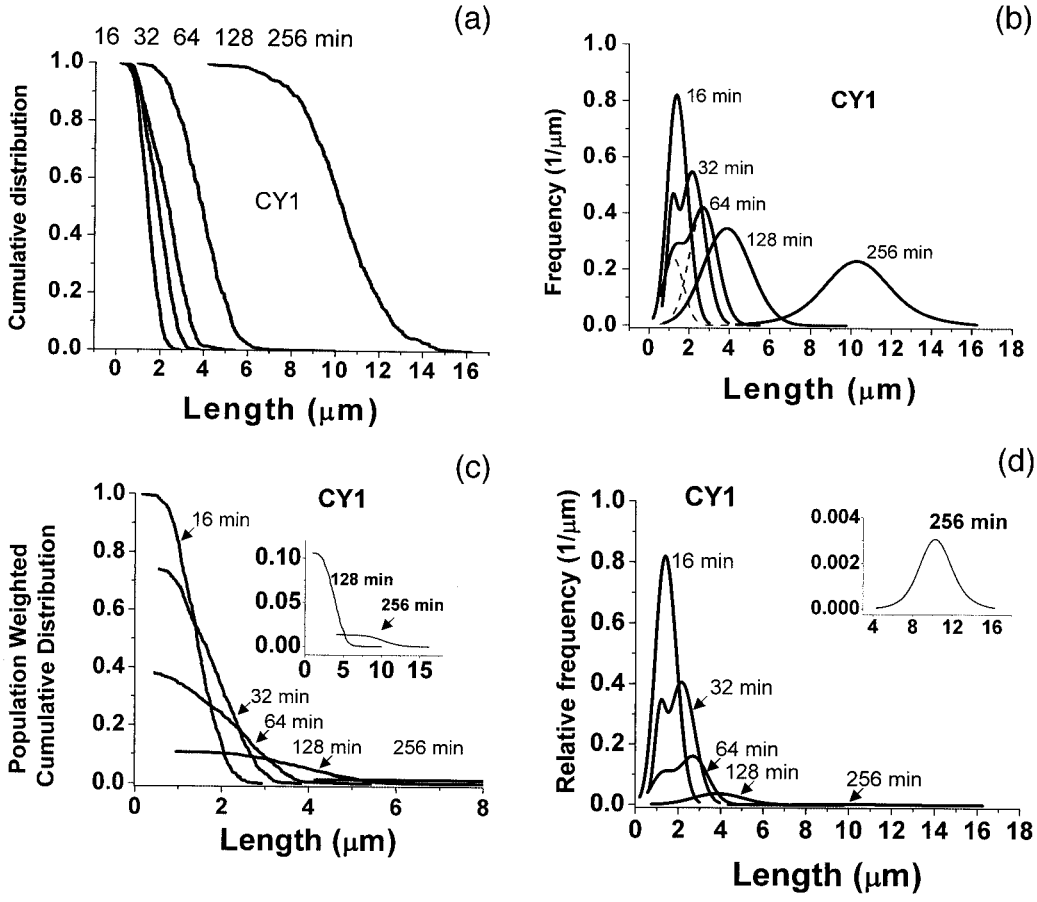

Fig. 1. (a) Cumulative distributions of crystal length for sample CY1 at different times. (b) Differential crystal length distributions derived from (a). Broken curves are two fitted Gaussian distributions that reproduce the distribution at 64 min. (c) Cumulative length distribution of (a) weighted by the total population (100% at 16 min). Inset shows two distributions at larger sizes in more detail. (d) Differential length distribution derived from (c). Inset shows distribution at 256 min in more detail.

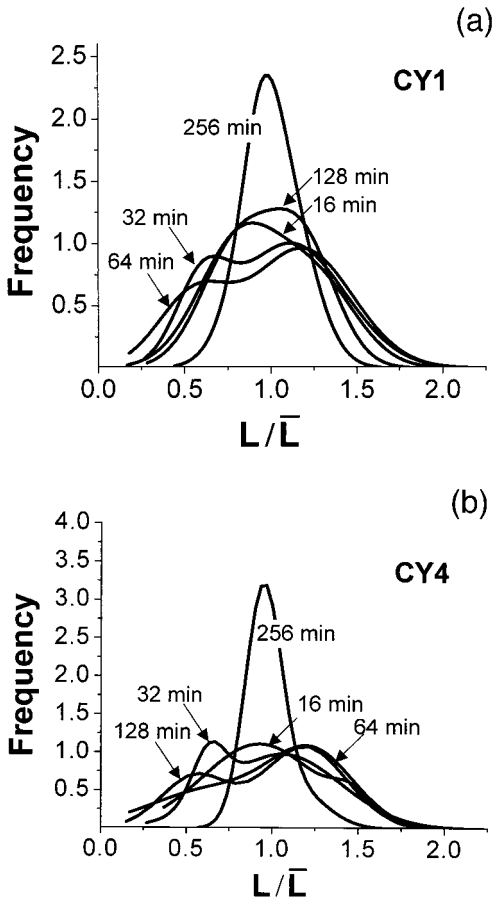

Fig. 2. Differential distribution against normalized length at different times. Evolving trends to develop skewing at different time and to sharpen at 256 min are similar in all compositions: (a) CY1 and (b) CY4.

To follow the shift of the distributions, we plot the mean length as a function of time in Fig. 3 for all four compositions. The observed feature is unlike that of a typical precipitation or coarsening reaction, in that, accelerated, rather than decelerated, growth/coarsening is found at the later time. Such late-stage acceleration gives a sigmoidal shape to the curves in Fig. 3. These features are further confirmed in the inset of Fig. 3 by plotting the near-maximum length of crystals (at 95 percentile) as a function of time. Again, acceleration instead of deceleration is found at later time.

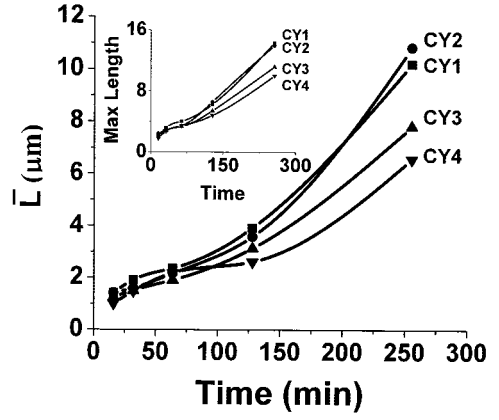

Fig. 3. Crystal length increases with time for all compositions. Shown in the main panel are data of average length and, in the inset, maximum length (at 95 percentile), using the same units. Note the sigmoidal feature of curves.

We now assume that the size is the only metric that determines the evolution of the crystals and that the crystal growth/shrinkage is by incrementally adding/subtracting mass and not by coalescence.[2] Then the population of crystals of one size group should exactly correspond to the population of another size group at a later time, with the size difference being the one caused by crystal growth/shrinkage. This correspondence can be applied to Fig. 1(c) at consecutive times to determine the corresponding groups, which are those points of the same F value but on different curves. This allows us to graphically determine the growth/shrinkage velocity. Mathematically, the above concept also can be expressed as a conservation condition for population, $dF = 0$, which holds as F evolves in size and with time. (This condition applies at all sizes except zero, where crystals disappear.) If the only size dimension of interest is length (the justification of this assumption is provided at the end of this section), then the full differential dF can be expressed in terms of partial differentials of length and time, which leads to

$$\frac{dL}{dt} = \frac{\partial F/\partial t}{\partial F/\partial L} \tag{1}$$

This equation is used to obtain the length velocity.

In the above equation, $\partial F/\partial L$ can be directly evaluated from Fig. 1(c) and is always negative. Referring to $\partial F/\partial t$, we also verify that there is a critical size, given by the intersection of two consecutive distributions, which satisfies $\partial F/\partial t = 0$ so there is no growth or shrinkage. It can be further seen that those crystals larger than the critical size satisfies $\partial F/\partial t > 0$ and, therefore, should grow, whereas those smaller than the critical size should shrink. The smallest crystals at an earlier time find no correspondence (of the same F value) at a later time; they are the crystals that have shrunk and disappeared during this time increment. These features provide a direct confirmation of coarsening kinetics: small crystals shrink and large crystals grow, while the total population decreases.

Analytically, to evaluate $\partial F/\partial t$, we have fitted the differential distribution using two Gaussian functions and recovered F by integration. We then interpolate the parameters of these Gaussian functions to estimate F at intermediate times, from which we can evaluate $\partial F/\partial t$. The velocity obtained from this analysis for CY1 is shown in Fig. 4. At any given time, the velocity initially increases with size and later decreases. As time progresses, the velocity–size curves gradually shift to the larger sizes. The maximum velocity initially decreases from 16 to 32 min, later increases from 64 to 128 min, and finally appears to decrease again from 128 to 256 min. Similar results are found for other compositions but are not shown here for brevity.

The width distributions also have been analyzed. The results are shown in Fig. 5 for CY4, but others are omitted. As in the case of length distributions, the normalized distributions of width experience an evolution of two Gaussian populations, and the distribution at 256 min is narrower than those at earlier times. The same features are observed for all other compositions although the narrowing at 256 min is not as sharp. The evolutions of mean width and near-maximum (95 percentile) width are shown in Fig.

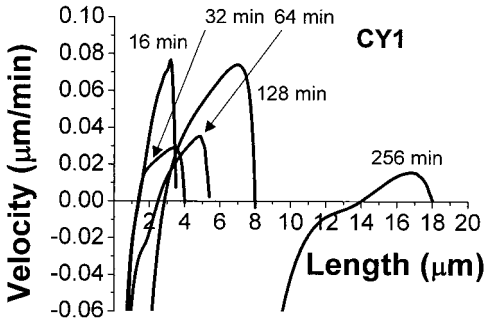

Fig. 4. Length velocity of CY1 as a function of crystal length at different times.

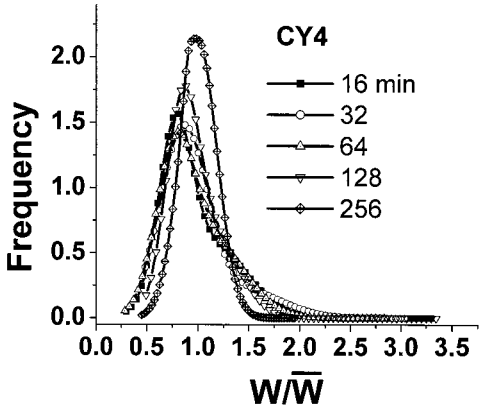

Fig. 5. Differential distribution against normalized width of CY4 at different times.

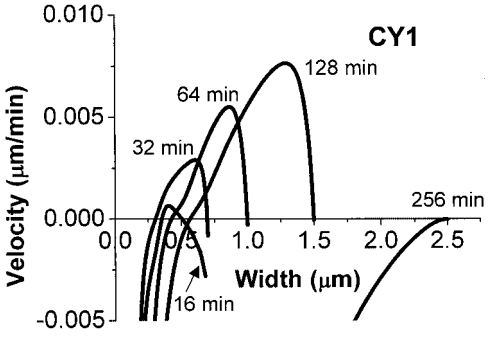

Fig. 7. Width velocity of CY1 as a function of crystal width at different times.

6 for all compositions. As in the case of length distributions, accelerated growth is observed. The width velocity of CY1 is plotted in Fig. 7 at different times. The velocity–size curves shift to the larger sizes, and the maximum velocity appears to increase through 128 min. (There are too few width data above 2.5 μm at 256 min; therefore, the velocity cannot be determined accurately.)

Because the sharpening of normalized size distribution is a rather unusual feature and has not been reported in the previous literature of particle growth and coarsening, we have further plotted in Fig. 8 for CY2 the normalized distribution of $(\text{volume})^{1/3}$, which is proportional to the (geometric-mean) linear dimension $(LW^2)^{1/3}$. A tendency to sharpen at the longest time is again observed. In connection to the mean linear dimension, we have previously shown (Fig. 4 of Part I) that it also undergoes accelerated growth at later time. We further show (Fig. 5 of Part I) that the crystal concentration decreases in a manner much steeper than $1/t$, which is the LSW prediction. All these observations are consistent with the accelerated coarsening found here.

Lastly, we examine the correlation between the length and the width of crystals. The crystals are first ranked by their length from long to short, then the widths of such ranked crystals are plotted in Fig. 9 for two times. For a monotonic length–width correlation, the ranking should be the same no matter whether length or width is used. In such a case, Fig. 9 should be a monotonic curve with no scatter. In reality, the distributions shown in Fig. 9 are scattered, and the scatter increases with time. Nevertheless, there is an overall trend of decreasing width with increasing ranking number, which implies a positive correlation between the width and the length. Therefore, a single size parameter, either length or width, suffices for the purpose of statistically ranking crystals at any given time. This correlation also provides the justification for using Eq. (1) to determine crystal velocity, because, statistically, length alone is sufficient to specify the size of a crystal.

IV. Accelerated Coarsening—The Role of β to β′ Transformation

Several important details of our experiments on the population dynamics of coarsening are not consistent with the prediction of the classical coarsening theories (LSW and its various modifications).[2–6] Most notably, all the previous theories predict that the coarsening velocity should decrease with time t, and the characteristic sizes (the mean, median, and maximum when there is a cut-off) should follow a power law t^n, with $n < 1$ (e.g., $n = 1/3$ if diffusion control and $n = 1/2$ if interface control, following the LSW theory). According to Fig. 4 of Part I and Figs. 3 and 6 here, however, the characteristic mean dimension, length, and width increase with time in a way inconsistent with $n < 1$. Rather, they apparently grow at an increasing rate. The velocity curves of different times, as displayed in Fig. 4, also appear to mostly shift to larger sizes without a significant decrease of overall rates. Indeed, some curves display a maximum velocity that increases with time. Such a behavior has not been reported in the literature of particle growth and coarsening.

The fundamental reason that the classical theories of coarsening predict a decreasing coarsening rate is that the driving force, which results from capillarity, decreases with particle size and, thus, with time. This conclusion is independent of whether the kinetics is diffusion controlled or interface controlled and whether the volume fraction of particles is very small or near unity (as in grain growth[15]). The chemical potential, which is responsible for such a

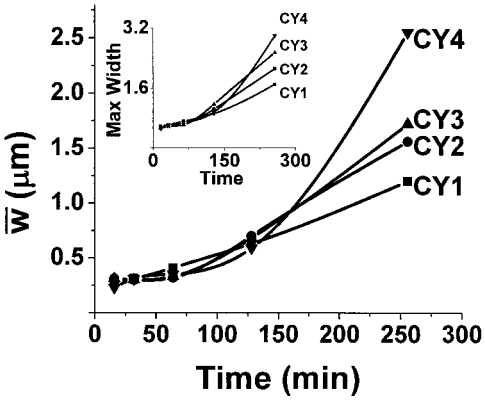

Fig. 6. Crystal width increases with time for all compositions. Shown in the main panel are data of average width and, in the inset, maximum width (at 95 percentile), using the same units.

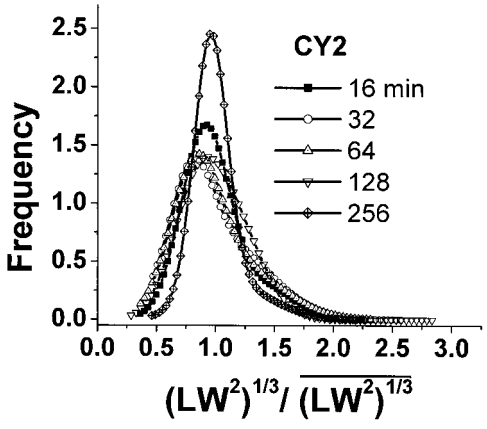

Fig. 8. Differential distribution against normalized linear length of CY2 at different times. Linear length is the geometric mean of length and squared width.

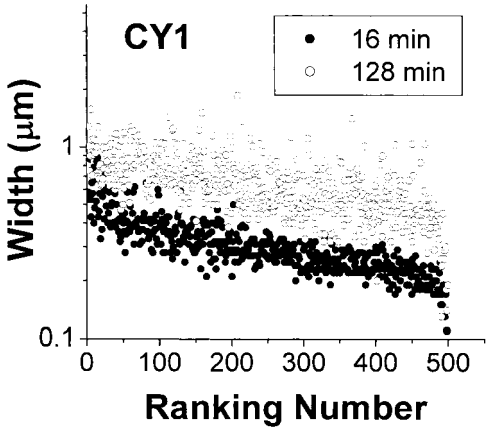

Fig. 9. Widths of 500 crystals first sorted in the order of decreasing length. Despite increasing scatter, a positive correlation between width and length is maintained.

driving force, which is the negative slope of the chemical potential, is illustrated in Fig. 10 (the upper left panel) for spherical particles of radius R, with an interfacial energy γ, and an atomic volume Ω. In our experiments, however, a phase transformation from β-Si_3N_4 to β′-SiAlON also occurs during coarsening.[1] The progression of this transformation is long and lasts essentially for most of, if not the entire, duration of our experiments (256 min). Clearly, it adds to the coarsening process a new driving force whose magnitude most likely overwhelms the driving force from capillarity.

As shown in Part I, the transformation is mostly a compositional transformation and does not involve a structural change; it mainly occurs by the replacement of Si–N bond by Al–O bond. (The relatively small volume increase caused by such replacement transformation is ignored here.) Because this transformation coincides with coarsening, it is likely that larger crystals are near the equilibrium composition of β′-$Si_2Al_4O_4N_4$, whereas the smaller crystals are closer to β-Si_3N_4. We therefore envision a phenomenological chemical potential that has an overall magnitude $\Delta\mu$ (the difference between the free energies, G_β for β-Si_3N_4 and $G_{\beta'}$ for β′-$Si_2Al_4O_4N_4$) but adopts an additional size dependence, as schematically shown in Fig. 10 in the lower left panel. (The sigmoidal shape of the size dependence is chosen to mimic the kinetics of a typical phase transformation of the Johnson–Mehl type.) It then follows that the driving force, which is obtained from the negative slope of the chemical potential, is largest at an intermediate size when the phase transformation is ~50% completed. This conclusion also stands for the overall driving force, because the slope of the overall chemical potential (the right panel of Fig. 10) has the same feature. Such a nonmonotonic size dependence of the driving force is a novel element that does not exist in the classical theories, in which the driving force always decreases with the particle size.

The above new feature is the cause of the unusual size kinetics and distribution evolutions observed in our experiments. Physically, as small crystals coarsen toward an intermediate size, accelerated growth due to the increasing driving force is expected. In our experiment, the transient time to reach this intermediate size is rather long, estimated to be >128 min, according to the XRD data of Part I. Therefore, accelerated coarsening should be manifest for much of the duration of our experiments. Later, when the crystals coarsen further to pass the intermediate size range, deceleration occurs, and the classical coarsening picture is recovered. Motivated by the above considerations, we have developed a theory for the coarsening kinetics under the above driving force.[14] We further note that the dissolution process probably involves no phase reversion (i.e., a shrinking β′ crystal does not transform to a β crystal.) Therefore, the kinetic pathway is not reversible and demands a numerical solution. We have simulated[14] the coarsening kinetics and shown that an initially Gaussian distribution of particles can evolve into a bimodal distribution because of the rapid growth of the larger particles, located at the knee of the combined curve in Fig. 10 (the right panel), which experience the maximum driving force. Later, when particles coarsen sufficiently, the driving force due to phase transformation becomes less important, which allows capillarity to restore a unimodal distribution that bares some resemblance to the distribution seen in classical coarsening. The simulation also shows that, initially, the particle size coarsens exponentially as the phase transformation sets in. Subsequently, when the average particle size exceeds the size of the maximum driving force for the phase transformation, the coarsening rate begins to decrease continuously. The simulation further predicts that the skewing of the size distribution should initially shift toward the smaller sizes, later toward the larger sizes, and finally toward the center, with a remarkable sharpening. All these predictions are in very good agreement with our experimental observations.

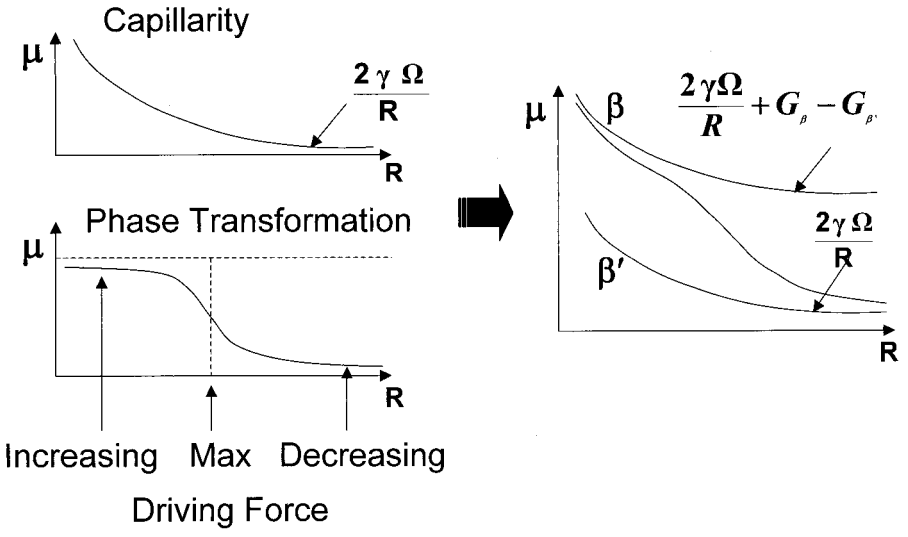

Fig. 10. Chemical potentials relevant for coarsening due to capillarity (upper left) and β to β′ phase transformation (lower left). Latter adopts a sigmoidal shape that is characteristic of the kinetics of the Johnson–Mehl type for many transformations. Driving force is obtained from the negative slope of these curves. In the combined chemical potential (the right panel), the driving force from the phase transformation is dominant, except at very small and very large sizes.

The above discussion ignores growth anisotropy. For diffusion problems involving the boundary condition of a constant chemical potential on the surface of an ellipsoid, it is well-known from potential theory that diffusion field outside the ellipsoid is formally the same as that outside a spherical surface, after a suitable canonical transformation.[16] Therefore, the kinetics of coarsening of a group of ellipsoidal particles of an identical aspect ratio should be similar to that of spherical particles. Growth anisotropy in Si_3N_4, however, is probably caused by different degrees of interface control on different crystal surfaces, which complicates the coarsening kinetics. Nevertheless, as discussed before, a decreasing coarsening rate should be expected according to the LSW theory no matter whether the kinetics is diffusion controlled or interface controlled. Therefore, the observation of accelerated coarsening in our experiments cannot be attributed to growth anisotropy or to disparities in interface control.

Lastly, although the existence of bimodal distribution in Fig. 2 may have the appearance of abnormal grain growth, abnormal grain growth is more often associated with the long tail of the distribution rather than a bimodal distribution with closely spaced local maximums, as in our case. Furthermore, the driving force for typical abnormal grain growth is the same as that for normal grain growth, namely capillarity. This is clearly not the case in our experiments at the intermediate time when bimodal distributions are most prominent.

V. Conclusions

(1) Contrary to the previous reports on Si_3N_4 ceramics, the t^n growth law (n ranging from 1/3 to 1/5) for crystal dimensions does not hold for liquid-grown crystals of a dilute volume fraction. Instead, there is strong evidence that the growth is qualitatively consistent with $n > 1$, implicating accelerated coarsening. This is despite the rapid decrease of crystal concentration, which falls much steeper than $1/t$, and the nearly constant total volume of crystals.

(2) Coarsening of Si_3N_4 in (Si,Al)(O,N) liquid is often concomitant with β-Si_3N_4 to β′-SiAlON transformation. Such transformation introduces an additional driving force for crystal dissolution and reprecipitation and, thus, accelerated coarsening. A recent analysis that incorporates this driving force into the coarsening kinetics produces results that are in good agreement with the observed crystal kinetics and population dynamics of our experiments.

(3) The above results are in part consistent with the previous study of Krämer *et al.*[13] of liquid-based crystal growth at 1640°C with a similar composition: little growth in the mean width during and after complete β-Si_3N_4 precipitation, but fast growth setting in at a later time. The more common observation of decelerated coarsening may still be possible when β to β′ transformation is complete and especially when impingement is severe, as in the case of ceramics.

Acknowledgment

This work was based on the Ph.D. dissertation of L.L.W. Helpful discussion with the members of the dissertation committee, Professor J. Halloran and Professor T. Pollock, is gratefully acknowledged.

References

[1]L. L. Wang, T. Y. Tien, and I-W. Chen, "Formation of β-Silicon Nitride Crystals from (Si,Al,Mg,Y)(O,N) Liquid: I, Phase, Composition, and Shape Evolution," *J. Am. Ceram. Soc.*, **86** [9] 1578–85 (2003).

[2]I. M. Lifshitz and V. V. Slyozov, "The Kinetics of Precipitation from Supersaturated Solid Solutions," *J. Phys. Chem. Solids*, **19** [1–2] 35–50 (1961).

[3]C. Wagner, "Theory of Precipitate Change by Redissolution," *Z. Electrochem.*, **65**, 581–91 (1961).

[4]A. J. Ardell, "The Effect of Volume Fraction on Particle Coarsening: Theoretical Considerations," *Acta Metall.*, **20** [1] 61–71 (1972).

[5]A. J. Ardell, "Precipitate Coarsening in Solids: Modern Theories, Chronic Disagreement with Experiment"; pp. 485–94 in *Phase Transformations '87*. Edited by G. W. Lorimer. The Institute of Metals, London, U.K., 1988.

[6]H. A. Calderon, P. W. Voorhees, J. L. Murray, and G. Kostorz, "Ostwald Ripening in Concentrated Alloys," *Acta Metall. Mater.*, **42** [3] 991–1000 (1994).

[7]R. D. Doherty, "Diffusive Phase Transformations in the Solid State"; pp. 1363–505 in *Physical Metallurgy*, 4th ed. Edited by R. W. Cahn and P. Haasen. Elsevier, New York, 1996.

[8]R. Wagner, R. Kampmann, and P. W. Voorhees, "Homogeneous Second-Phase Precipitation"; pp. 309–407 in *Phase Transformations in Materials*. Edited by G. Kostorz. Wiley–VCH, New York, 2001.

[9]C. M. Hwang, T. Y. Tien, and I-W. Chen, "Anisotropic Grain Growth in Final Stage Sintering of Silicon Nitride Ceramics"; pp. 1034–39 in *Sintering '87, Proceedings of 4th International Symposium on Science and Technology of Sintering*, Vol. 2. (Nov. 4–7, 1987, Tokyo, Japan). Edited by S. Somiya, M. Shimada, M. Yoshimura, and R. Watanabe. Elsevier, New York, 1988.

[10]C. M. Hwang and T. Y. Tien, "Microstructure Development in Silicon Nitride Ceramics," *Mater. Sci. Forum*, **47**, 84–109 (1989).

[11]K.-R. Lai and T. Y. Tien, "Kinetics of β-Si_3N_4 Grain Growth in Si_3N_4 Ceramics Sintered under High Nitrogen Pressure," *J. Am. Ceram. Soc.*, **76** [1] 91–96 (1993).

[12]M. Krämer, M. J. Hoffmann, and G. Petzow, "Grain Growth Kinetics of Si_3N_4 during α/β-Transformation," *Acta Matall. Mater.*, **41** [10] 2939–47 (1993).

[13]M. Krämer, M. J. Hoffmann, and G. Petzow, "Grain Growth Studies of Silicon Nitride Dispersed in an Oxynitride Glass," *J. Am. Ceram. Soc.*, **76** [11] 2778–84 (1993).

[14]I-W. Chen, A. Davenport, and L.-L. Wang, "Accelerated Precipitate Coarsening due to a Concomitant Secondary Phase Transformation," *Acta Mater.*, **51** [6] 1691–703 (2003).

[15]M. Hillert, "On the Theory of Normal and Abnormal Grain Growth," *Acta Metall.*, **13** [3] 227–38 (1965).

[16]W. R. Smythe, *Static and Dynamic Electricity*, 3rd Ed.; pp. 123–26. McGraw-Hill, New York, 1968. □